



**HAL**  
open science

## Effects of Ag or Si on precipitation in the alloy Al-2.5% Cu-1.5% Mg

Anne-Marie Zahra, Christian Zahra, Myriam Dumont

► **To cite this version:**

Anne-Marie Zahra, Christian Zahra, Myriam Dumont. Effects of Ag or Si on precipitation in the alloy Al-2.5% Cu-1.5% Mg. Philosophical Magazine, 2005, 85 (31), pp.3735-3754. 10.1080/14786430500278924 . hal-00513595

**HAL Id: hal-00513595**

**<https://hal.science/hal-00513595v1>**

Submitted on 1 Sep 2010

**HAL** is a multi-disciplinary open access archive for the deposit and dissemination of scientific research documents, whether they are published or not. The documents may come from teaching and research institutions in France or abroad, or from public or private research centers.

L'archive ouverte pluridisciplinaire **HAL**, est destinée au dépôt et à la diffusion de documents scientifiques de niveau recherche, publiés ou non, émanant des établissements d'enseignement et de recherche français ou étrangers, des laboratoires publics ou privés.



**Effects of Ag or Si on precipitation in the alloy Al-2.5% Cu-1.5% Mg**

Journal:	<i>Philosophical Magazine &amp; Philosophical Magazine Letters</i>
Manuscript ID:	TPHM-05-Feb-0038.R2
Journal Selection:	Philosophical Magazine
Date Submitted by the Author:	25-Jul-2005
Complete List of Authors:	ZAHRA, Anne-Marie; Faculty of Science, TECSSEN/CNRS ZAHRA, Christian; Faculty of Science, TECSSEN/CNRS DUMONT, Myriam; Université Paul Cézanne - Aix-Marseille III, TECSSEN-UMR6122
Keywords:	clusters, calorimetry, aluminium alloys, age-hardening
Keywords (user supplied):	GPB zones



# Effects of Ag or Si on precipitation in the alloy Al-2.5 % Cu-1.5 % Mg

A.-M. ZAHRA, C.Y. ZAHRA and M. DUMONT<sup>+</sup>

Université Paul Cézanne – Aix-Marseille III

Thermodynamique, propriétés Electriques, Contraintes et Structures aux Echelles

Nanométriques (TECSEN), UMR 6122, CNRS,

Faculté des Sciences et Techniques de St. Jérôme,

Case 261, 13397 Marseille cedex 20, France

<sup>+</sup> Corresponding author. Email: myriam.dumont@univ.u-3mrs.fr

## ABSTRACT

Calorimetric measurements and electron microscopy observations were performed on Al-2.5 mass% Cu-1.5 mass% Mg alloys containing also 0.4, 1 or 2 % Ag or 0.5 % Si, in order to improve understanding of the relationships between precipitation processes and age hardening. The analogous behaviour of calorimetric and hardness data confirms that the first hardening stage is initiated in all alloys by GPB zone formation which occurs via a nucleation and growth controlled mechanism. The vacancy-trapping effect of Mg is increased by Ag and Si additions and leads to slower precipitation kinetics. Consequently refined GPB zones sizes are obtained leading to an increase in hardness with respect to the ternary alloy. During the second hardening stage, the formation of the more stable S' phase increases the total amount of strengthening precipitates in the ternary alloy. Phases typical for binary Al-Cu alloys form additionally in the Si-containing alloy. In the Ag-bearing alloys, precipitation of the hardening X' phase occurs the earlier the higher the Ag content is; it is followed by S' precipitation. During heating of the ternary alloy, the S' phase forms after substantial dissolution of GPB zones and of the S'' phase identified by high resolution electron microscopy; this contradicts the concept of a continuous precipitation sequence.

Key words: aluminium alloys, age-hardening, calorimetry, clusters, GPB zones

## 1. Introduction

The precipitation processes in Al-Cu-Mg alloys which fall within the ( $\alpha + S$ ) region of the ternary phase diagram [1] have been the subject of numerous research due to their fundamental and commercial interest since the discovery of the alloy duralumin in

1  
2  
3 1906. Since then they have been studied mainly by mechanical testing, calorimetric  
4 measurements and electron microscopy observations. Two hardness stages are  
5  
6 observable during ageing at medium temperatures [2,3]; a rapid initial rise which may  
7  
8 account for 50 to 70 % of the total hardness increase, and a second rise, much slower  
9  
10 than the first one. In semi-logarithmic representation, they are separated by a sort of  
11  
12 plateau whose duration depends strongly on temperature and alloy composition. In  
13  
14 normal scale, a plateau does not always appear [4].  
15  
16  
17  
18  
19

20 More recently, atom probe field ion microscopy (APFIM), positron annihilation  
21 spectroscopy (PAS) and high resolution transmission electron microscopy (HRTEM)  
22 were applied to the study of these alloys; some of the results obtained with these new  
23 techniques are in contradiction with conclusions of earlier work.  
24  
25  
26  
27  
28

29 a - The first controversy concerns the state of the solid solution (SS). X-ray and  
30 thermodynamic data indicate a clustering tendency between the Cu atoms in Al-Cu [5]  
31 and the Mg atoms in Al-Mg alloys [6] as well as a strong interaction between the Cu  
32 and Mg atoms in ternary alloys (e.g. [7]). However, it was concluded from three-  
33 dimensional atom probe (3D-AP) analyses on an Al-2.5 mass% Cu-1.5 mass% Mg alloy  
34 [8] that the solute atoms are still uniformly distributed after 1 min hold at 150 or 200  
35 °C. Computer simulations of the decomposition process in these alloys also start from  
36 random atomic configurations in SS [9].  
37  
38  
39  
40  
41  
42  
43  
44  
45  
46  
47

48 b - Disagreement also exists to explain the rapid decomposition after quenching  
49 leading to the first hardening stage. It is attributed either to the formation of Guinier-  
50 Preston-Bagaryatsky (GPB) zones (e.g. [3, 10-12]) or to solute atom clustering [13-16]  
51 or to solute atom-dislocation interactions [8] or to the presence of dislocation loops  
52 resulting from quenched-in vacancies [17]. The formation of GPB zones during ageing  
53 at temperatures as low as room temperature (RT) was deduced from X-ray [10],  
54  
55  
56  
57  
58  
59  
60

1  
2  
3 hardness [18] and calorimetric [19,20] measurements but remains undetected by  
4  
5 HRTEM due to their extremely small sizes (around 1 nm), hence is not accepted  
6  
7  
8 universally. The zones are considered to be cylindrical [10], mono- [20] or multilayered  
9  
10 [21]. Besides, three-dimensional clusters visible by HRTEM after ageing at medium  
11  
12 temperatures (e.g. 500h at 150°C) are designated by some authors as GPB zones  
13  
14 [14,15]; energy dispersive X-ray spectroscopy (EDS) analyses performed on an Al-  
15  
16 2.5% Cu-1.5% Mg-0.1% Si alloy (Mg:Cu atomic ratio of 1.5) and aged for 14 h at  
17  
18 200°C, show clusters enriched in Mg but not in Cu with respect to the matrix [22].  
19  
20 Hence they might correspond to the Mg-rich clusters observed by Charai *et al.* [20] in a  
21  
22 ternary alloy of similar ratio aged for 4 h at 200 °C. Clusters which are in most cases  
23  
24 richer in Cu than in Mg, were found at 150 °C for Mg:Cu ratios of 0.4 and 1 [23]. All  
25  
26 these clusters are characterised by a very high Al content of about 90% [23-25] and  
27  
28 contain vacancies. Cu-Mg clusters detected by APFIM are considered to act as  
29  
30 nucleation sites for GPB zones which precipitate only during the second stage of  
31  
32 hardening [13,15,26].  
33  
34  
35  
36  
37

38  
39 c - The existence of a coherent S'' phase (or GPBII), analogous to θ'' (or GPII) in  
40  
41 Al-Cu alloys, is also highly discussed. Recent simulations of Wang and Starink [27]  
42  
43 based on an orthorhombic structure of composition  $Al_{10}Cu_{3+x}Mg_{3-x}$  ( $0 \leq x \leq 1$ ) match the  
44  
45 electron microscopy image and diffraction pattern of Charai *et al.* [20]. According to  
46  
47 Shih *et al.* [28], S'' is identical to partially ordered GPB zones; according to Ringer *et al.*  
48  
49 [26], S'' is a variant of S.  
50  
51  
52

53  
54 d - There is no unanimity whether the orthorhombic metastable S' phase should be  
55  
56 distinguished from the orthorhombic stable S phase ( $Al_2CuMg$ ) or not [13]. The  
57  
58 metastable character of S' is linked to Cu:Mg ratios different from unity. Charai *et al.*  
59  
60 [20] observed slight differences between S' and S in calorimetric and HRTEM studies

1  
2  
3 and proposed that, during the gradual evolution from  $S'$  to  $S$ , the lattice parameters of  $S'$   
4 vary with size (degree of coherency) until they reach the values for the stable phase  $S$   
5  
6 which is non-coherent with the matrix. Nucleation of  $S'$  is fairly independent of GPB  
7 zones (e.g. [29,13]) but is proposed to start from clusters [30] dominantly rich in Mg, if  
8 the alloy has a Mg:Cu ratio of 1.6 [20]. This is seemingly supported by HRTEM studies  
9  
10 [31,22], although clusters are considered to be GPB zones on which  $S$  (or  $S'$ ) particles  
11 may nucleate. Based on HRTEM, Radmilovic *et al.* [32] recently proposed a new model  
12 for the crystalline structure of the incoherent  $S$  phase which was criticised for energetic  
13 reasons [33].  
14  
15  
16  
17  
18  
19  
20  
21  
22  
23  
24

25 e - The precipitation sequence operative in  $(\alpha + S)$  alloys remains uncertain. The  
26 following one is most often cited [34] for decomposition from the supersaturated solid  
27 solution (SSSS):  
28  
29  
30  
31



33  
34 A shorter one is derived from ageing studies at 150 °C [13] :



36  
37 A two-stage sequence was introduced by Charai *et al.* [20] for alloys with Mg:Cu  
38 ratios around 1.6 :  
39  
40  
41  
42



45  
46 In agreement with APFIM studies (e.g. [26]), GPB zones are considered to  
47 nucleate from Cu-rich clusters and may transform into  $S''$ ; only after substantial but not  
48 complete dissolution of  $S''$ , solute atoms may combine with residual clusters enriched in  
49 Mg and form the  $S'$  phase which gradually approaches the composition  $\text{Al}_2\text{CuMg}$  by  
50 decreasing the solubility of Cu and Mg in Al towards their equilibrium values. Hence  
51 the fraction precipitated increases and may induce a new (second) hardness rise [11].  
52  
53  
54  
55  
56  
57  
58  
59  
60

1  
2  
3 The precipitation kinetics of GPB zones and S' are slowed down by increasing the  
4 concentration in Mg atoms which trap vacancies preferentially and hinder the diffusion  
5 of Cu atoms [3,12].  
6  
7  
8  
9

10 f - The influence of small Ag or Si additions to Al-Cu-Mg alloys was already  
11 examined several times but results are contradictory. GPB zone formation is mostly  
12 reported to be slowed down [3,18,22,35,36], whereas it is expected to be accelerated  
13 according to computer calculations [9]. At medium temperatures, a new and probably  
14 initially coherent phase, X', appears in Ag-containing alloys [37]. This phase nucleates  
15 on sites of Mg-Ag co-clusters, forms hexagonal platelets on {111} matrix planes and  
16 approximates the composition of S with up to 5 at% Ag [15]. In Si-bearing alloys, S'  
17 formation is found to be either enhanced [38] or retarded [35,36].  
18  
19  
20  
21  
22  
23  
24  
25  
26  
27  
28  
29

30 The aim of the present work is to resolve as many discrepancies as possible by  
31 carrying out calorimetric measurements and some phase characterizations by HRTEM  
32 on the same alloys as those used in many previous investigations [3,13-  
33 15,18,22,26,37,39,40] and by referring to existing hardness data and electron  
34 microscopy observations. Calorimetry is of special interest for studies involving  
35 nanometer sized precipitates which are difficult (and in many cases still impossible) to  
36 detect by direct methods. Moreover, heat flow calorimetry enables to measure the  
37 kinetics of a process over several days (weeks) and informs on the reaction mechanism.  
38  
39  
40  
41  
42  
43  
44  
45  
46  
47  
48  
49  
50

## 51 **2. Experimental**

52 Five alloys were investigated in the shape of 1 mm thick specimens; their compositions  
53 (except for alloy 5 used by Hutchinson and Ringer [22]) were determined by inductively  
54 coupled plasma atomic absorption spectroscopy and are given in Table 1 in mass and  
55 atomic %; the uncertainty is estimated to  $\pm 0.1\%$  for Cu and Mg. All these alloys were  
56  
57  
58  
59  
60

1  
2  
3 solutionised for 1h at 500°C, quenched into water at RT and analysed in this state or  
4  
5 aged beforehand at temperatures between RT and 200 °C for specified times. The Ag  
6  
7 concentration in alloy 4 is still soluble at 500°C, as can be concluded from the  
8  
9 mechanical properties [18] and DSC studies (present work) of alloys containing up to  
10  
11 2% Ag. In fact, hardness increases steadily with Ag content and surpasses the ternary  
12  
13 alloy [18]. DSC runs show that even during heating at 20 K min<sup>-1</sup>, complete  
14  
15 redissolution of the precipitates is achieved at 500 °C except in the alloy with the  
16  
17 highest Ag content in which some concentration inhomogeneities persist up to 530 °C  
18  
19 (see figure 3).  
20  
21  
22  
23  
24

25 Table 1 : Alloy compositions in mass % (at.%)

	Cu	Mg	Ag	Si
Alloy 1	2.5 (1.1)	1.5 (1.7)	<0.001	<0.01
Alloy 2	2.5	1.5	0.4 (0.1)	<0.01
Alloy 3	2.5	1.5	1.0 (0.25)	<0.01
Alloy 4	2.5	1.5	2.0 (0.5)	<0.01
Alloy 5	2.5	1.5	<0.001	≈0.5

26  
27  
28  
29  
30  
31  
32  
33  
34  
35  
36  
37  
38  
39  
40  
41  
42  
43 Fe : 0.03

Zn < 0.005

Zr < 0.005

Mn < 0.01

Cr < 0.005

Sr < 0.001

Ni < 0.01

Ti < 0.005

Al balance

44  
45  
46  
47  
48 Isothermal calorimetric measurements were carried out at 30, 150 and 180°C with  
49  
50 the help of Tian-Calvet heat conduction calorimeters measuring the heat flow, dH/dt,  
51  
52 versus time. Hence these calorimetric curves give directly the isothermal reaction  
53  
54 kinetics. Curves which display a heat flow minimum are typical for reactions involving  
55  
56 nucleation and growth mechanisms and yield sigmoid-shaped curves when plotting the  
57  
58 heat evolved (obtained by integrating heat flows) or the fraction transformed (e.g. [41].)  
59  
60



1  
2  
3 Twenty specimens of each alloy, 1 mm thick and 15 mm in diameter, are used to  
4 perform isothermal calorimetry experiments. The time elapsed between quenching of  
5 the specimens, drying and transfer into the calorimeter after preheating to a temperature  
6 slightly higher than that of the apparatus is about 5 min. As the parasitic heat effects due  
7 to the introduction into the calorimeter last for about 30 min in spite of preheating,  
8 curves are not quantitative for times < 30 min, but their relative importance is respected  
9 when assuring identical conditions for introduction (which are chosen in such a way that  
10 introduction of pure Al specimens of the same mass gives exothermic effects; see figure  
11 1). Specimens were examined either directly after quenching or after pre-ageing at RT  
12 in order to assess the influence of pre-ageing on the precipitation kinetics of more stable  
13 phases.  
14  
15  
16  
17  
18  
19  
20  
21  
22  
23  
24  
25  
26  
27  
28

29 Differential scanning calorimetry (DSC) was performed with a power-  
30 compensated thermal analyser (Perkin-Elmer DSC7) which measures heat flows as a  
31 function of temperature. All experiments were done at a heating rate of  $20 \text{ Kmin}^{-1}$  for  
32 which corrections for thermal inertia are small [42] and were neglected. In general, each  
33 experiment was repeated twice on quenched as well as on aged alloys. Base line  
34 corrections for drift which increases with temperature were done with the help of  
35 polynomial equations. The first 3 min are lost due to operation and temperature  
36 stabilisation of the specimen.  
37  
38  
39  
40  
41  
42  
43  
44  
45  
46  
47

48 Thin foils for the electron microscopy studies were prepared by twin jet  
49 electropolishing at 250 K using a mixture of 33% nitric acid and 67% methanol. They  
50 were examined in a Jeol 2010 F, UPR 22 microscope having a spatial resolution of 0.19  
51 nm. This instrument is located at the Centre Pluridisciplinaire de Microscopie  
52 électronique et de Microanalyse of the Faculty of Science.  
53  
54  
55  
56  
57  
58  
59  
60

### 3. Results and interpretation

#### 3.1. Isothermal studies

**3.1.1. Ageing at 30 °C.** When isothermally aged at 30 °C (figure 1), all alloys show a heat flow minimum which is situated at about 0.5 h for alloy 1 (not visible at the scale chosen), 1.7 h for alloy 5, 3 h for alloy 2 and 11 h for alloy 3. Due to uncertain extrapolation to zero time, the respective heats cannot be distinguished but lie all within  $-(13.5 \pm 1.5)$  J/g when integrating between 30 min and 4 days (d). These relatively high values are characteristic for the formation of a metastable/stable phase, presumably GPB zones, via a nucleation and growth process [41].

[Insert fig. 1]

**3.1.2. Ageing at 150 and 180 °C.** When aged at 150 °C (the corresponding curves are not reproduced), alloys 1 and 5 show an overlap of two exothermic reactions, a strong one which decays over the first day and a much weaker and slower one which forms a flat minimum after several days and was attributed to S' formation [20]. It is attained around 9.5 days in alloy 1 but is still not reached after 14 days of experiment for alloy 5. Only falling heat flows corresponding to growth processes are recorded for alloys 2 and 3.

[Insert fig. 2]

Curves obtained at 180 °C, given in figure 2, show a more rapid kinetic evolution than at 150 °C. It is proposed that after partial GPB zone dissolution (initial endothermic effects which last longer in pre-aged samples), the main exothermic peak in alloy 1 (curve 1) represents S' formation via a nucleation and growth controlled mechanism and its gradual transformation into S. As its heat value,  $-(12.5 \pm 1)$  Jg<sup>-1</sup>, is lower than the value obtained by DSC (§3.2.), it has to be concluded that another phase,

1  
2  
3 probably  $S''$  formed from GPB zones, dissolves simultaneously at longer ageing times.  
4  
5  
6 In fact, the presence of the  $S''$  and  $S'$  phases after 15 h ageing at 180 °C was confirmed  
7  
8 by electron microscopy (§3.3) and DSC (curve similar to the one obtained after 4 h at  
9  
10 200 °C in figure 7(a)). Precipitation of the  $S'$  phase in a similar alloy aged at 190 °C has  
11  
12 also been observed by TEM [35].  $S'$  precipitation is reinforced by pre-ageing at RT  
13  
14 (curve 1a) and, to a lesser extent, at 100 °C (curve 1b). However, no changes in the heat  
15  
16 value or in the time position of the maximum rate of transformation are observed as  
17  
18 compared to the water quenched sample. This suggests that pre-ageing influences the  
19  
20 nucleation process by changing the number of nuclei and/or defects (dislocation loops  
21  
22 and helices) but not the rate of  $S'$  growth via Cu atom diffusion. The shape and relative  
23  
24 position of the curves 1a and 1b exclude important direct transition of bigger GPB zones  
25  
26 and/or  $S''$  particles into  $S'$  avoiding nucleation problems.  
27  
28  
29  
30  
31  
32

33 The Si addition in alloy 5 induces a slower rate of the major precipitation process  
34  
35 at 180 °C (figure 2, curve 5) as compared to alloy 1. The asymmetry of the peak  
36  
37 indicates the presence of two overlapping subpeaks; they are ascribed to  $\theta'$  and  $S'$   
38  
39 formation, as the alloy composition is close to the ( $\alpha + S + \theta$ ) field [22]. Pre-ageing at  
40  
41 low temperatures (curve 5a) has a retarding effect on precipitation; DSC measurements  
42  
43 performed on specimens aged for 1 d at 180 °C with and without 7 d hold at RT confirm  
44  
45 that the overall precipitation is indeed less advanced after pre-ageing.  
46  
47  
48  
49  
50  
51

## 52 **3.2. DSC studies**

53  
54 **3.2.1. As-quenched state.** Figure 3 summarises the heat flow curves obtained when the  
55  
56 quenched alloys undergo continuous heating up to 550 °C; note again that the first 3  
57  
58 min are lost.  
59  
60

1  
2  
3 The behaviour of alloy 1 is comparable to that of an Al-2 mass% Cu-1.3 mass% Mg  
4 alloy investigated by Charai *et al.* [20] and was interpreted as follows:  
5  
6

- 7  
8 ■ formation of GPB zones (peak around 80 °C amounting to about -8.5 Jg<sup>-1</sup>),  
9
- 10 ■ dissolution of GPB zones (around 200 °C) and partial transformation into S''  
11 (overlapping exothermic peak around 220 °C),  
12
- 13 ■ S'' dissolution around 250 °C,  
14
- 15 ■ precipitation of S' (peak around 290 °C) partly overlapping with S'' dissolution,  
16 partial transformation of S' into S (peak asymmetry)  
17
- 18 ■ finally dissolution of S' and S accompanied by a heat value of 17 Jg<sup>-1</sup> before  
19 reaching the high temperature SS around 480 °C.  
20  
21  
22  
23  
24  
25  
26

27  
28 It was observed [20] that in quenched and RT aged alloys, S'' is formed during the DSC  
29 analysis from GPB zones, whereas, when aged at higher temperatures or longer times, it  
30 is formed preliminary to the DSC scan (hence the exothermic heat flows accompanying  
31 GPB zones → S'' transformation become increasingly smaller). The same interpretation  
32 is adopted for alloy 1, as the presence of the S'' phase is confirmed in the present study  
33 (§3.3).  
34  
35  
36  
37  
38  
39  
40  
41

42 [Insert fig. 3]

43  
44 A heat balance shows that the decomposition of the SSSS starts immediately after  
45 quenching of alloy 1 and involves a heat loss of about 2 Jg<sup>-1</sup> before DSC analysis. In  
46 alloys 2-5, such a heat loss is less noticeable. For alloy 5, heat values for GPB zone  
47 formation on one hand and S' (S) formation or dissolution on the other hand are about  
48 10 and 16 J/g respectively, with an uncertainty of ±1 Jg<sup>-1</sup>. GPB zone formation  
49 enthalpies obtained during heating at 20 Kmin<sup>-1</sup>, when compared to values determined  
50 from isothermal calorimetry, are smaller; in fact, long-time isothermal ageing enables  
51 more important growth. On the contrary, S' formation enthalpies obtained during  
52  
53  
54  
55  
56  
57  
58  
59  
60

1  
2  
3 continuous heating are higher than values from isothermal calorimetry, as S'' dissolution  
4 overlaps much less. The most interesting result concerns the beginning of GPB zone  
5  
6  
7 formation: it is shifted to higher temperatures (i.e. retarded) when going from alloy 1 to  
8  
9 alloys 5, 2 and 4. The GPB peak temperatures shift in the same order.

10  
11  
12 In the Ag-containing alloys 2 and 4, two small exothermic peaks appear at  
13  
14 medium temperatures (around 250 and above 300 °C) instead of the strong and  
15  
16 asymmetric one in alloys 1 and 5; they are separated by a very small endothermic peak.  
17  
18 An increasing Ag content moves the exothermic effects to lower temperatures. The first  
19  
20 peak is attributed to the formation of the X' phase, since this phase was identified by  
21  
22 electron microscopy in alloy 2 aged for 1 h at 240 °C [37]. The second exothermic peak  
23  
24 is presumably associated with the precipitation of S', as the peak temperature of alloy 4  
25  
26 is close to the S' formation peak of the ternary alloy 1. In alloy 2, X' precipitates later  
27  
28 than in alloy 4 hence starts to dissolve later. The corresponding endothermic effects  
29  
30 overlap more substantially the S' exotherm whose peak temperature no longer  
31  
32 corresponds to its highest precipitation rate.  
33  
34  
35  
36  
37  
38

39  
40 The Si content in alloy 5 exceeds the solubility limit which approximates 0.1% at  
41  
42 520 °C according to Hutchinson and Ringer [22]; hence Mg<sub>2</sub>Si precipitates are expected  
43  
44 to be present after quench and their volume fraction should increase during ageing at  
45  
46 200 °C [22]. This may provoke the small exothermic effect observed around 180 °C  
47  
48 which overlaps with GPB zone dissolution in figure 3, as well as the small dissolution  
49  
50 effect before reaching the SS due to its increased solubility in this temperature range.  
51  
52 Another interpretation would be that the three endotherms >145 °C correspond to the  
53  
54 successive dissolution of zones typical for Al-Mg-Si alloys present in a small amount,  
55  
56 GPB zones and the S''-phase.  
57  
58  
59  
60

1  
2  
3 **3.2.2. Ageing at RT after quenching or reversion.** Curves obtained after several  
4 months of ageing at RT are given in figure 4. GPB zone dissolution starts at  
5 increasingly higher temperatures when going from alloy 4 to 2, 5 and 1; this reflects  
6 greater zone sizes which necessitate higher reversion temperatures. The overlapping  
7 exothermic effects  $>130\text{ }^{\circ}\text{C}$  and  $>150\text{ }^{\circ}\text{C}$  well visible in the Ag-containing alloys 4 and  
8 2, respectively, may be due to new zones precipitating during the DSC scan, such as in  
9 the case of alloy 1 aged for shorter times (figure 5).

10  
11  
12  
13  
14  
15  
16  
17  
18  
19  
20 If alloy 1 spends 3 h at RT before the DSC scan (figure 5, curve a), some GPB  
21 zones precipitate during the DSC scan from the still SSSS around  $100\text{ }^{\circ}\text{C}$ ; they get  
22 partially dissolved during further heating but new zones appear for temperatures higher  
23 than  $150\text{ }^{\circ}\text{C}$ , as can be deduced from the overlapping exothermic peak. This peak is still  
24 visible after 7 h ageing (curve b) but absent after ageing for times  $\geq 1$  day (curve c). This  
25 was attributed to the retention of excess vacancies enabling size evolution during  
26 heating [43]. When increasing the ageing time at RT after quenching, the S'  
27 precipitation peak in the subsequent DSC scans become increasingly sharper; their start  
28 and peak temperatures are lower than after quenching (cf. curves a and c in figure 5 and  
29 curves 1 in figures 3 and 4).

30  
31  
32  
33  
34  
35  
36  
37  
38  
39  
40  
41  
42  
43  
44 [Insert figs. 4 and 5]  
45

46  
47 When most of the excess vacancies are eliminated by a 4 min hold at  $230\text{ }^{\circ}\text{C}$  after  
48 quenching, GPB zone formation is extremely slow at RT (no measurable heat flow in a  
49 calorimeter at  $30\text{ }^{\circ}\text{C}$ ) but becomes visible for temperatures higher than  $100\text{ }^{\circ}\text{C}$  during a  
50 DSC run at  $20\text{ K/min}$  (figure 5, curve d); the S' formation peak starts a bit earlier than  
51 after water quenching and its heat value is not well reproducible, probably due to some  
52 initiation of S' precipitation during short holding at  $230\text{ }^{\circ}\text{C}$ . RT ageing after reversion  
53  
54  
55  
56  
57  
58  
59  
60

1  
2  
3 has little influence on the shape and temperature position of the S' peak (hence curves  
4 are not reproduced).  
5  
6  
7  
8  
9

10 **3.2.3. Ageing at 150 °C.** Figures 6(a) and 6(b) display DSC curves obtained for alloy 1  
11 and 2, respectively, aged for specified times at 150 °C before DSC analyses (note the  
12 different ordinate scale). It appears that a 10 min hold is sufficient to involve significant  
13 GPB zone formation (also observed for alloys 3, 4 and 5); their sizes (i.e. stability  
14 against heating) increase when passing from alloy 4 to 2, 5 and 1, just as after RT  
15 ageing. In alloy 1 (see figure 6(a)), the amount of S'' (endothermic peak around 255 °C)  
16 decreases after about 1 day in favour of S' formation reflected by progressively  
17 decreasing S' peaks during the subsequent DSC scans; this time corresponds to the  
18 second hardness rise [3,18]. The curve obtained after 3 months of ageing indicates that  
19 the phases S'', S' and S co-exist; their dissolution enthalpy amounts to 25 J/g. Pre-ageing  
20 for 8 days at RT before 1 day ageing at 150 °C (curve PA) promotes the transformation  
21 of GPB zones into S'' (smaller GPB zone and earlier S'' dissolution peaks); it also leads  
22 to a much sharper S' precipitation peak, hence to a narrower S' size distribution than  
23 after direct ageing for 1 day at 150 °C.  
24  
25  
26  
27  
28  
29  
30  
31  
32  
33  
34  
35  
36  
37  
38  
39  
40  
41  
42  
43

44 [Insert figs. 6(a) and (b)]  
45  
46

47 Increasing the ageing time of alloy 2 at 150 °C from 1 h (start of second hardening  
48 stage according to Vietz and Polmear [3]) to 1 day increases the importance of the  
49 second endothermic peak in figure 6(b) which overlaps GPB zone dissolution and is  
50 attributed to S'' dissolution; the X' formation peak around 250 °C becomes slightly  
51 reduced. Between 1 and 4 days, the amount of S'' decreases and that of X' increases  
52 strongly; S' appears as well (leading to a reduction of the X' and S' peaks during  
53 subsequent analyses). After 3 months ageing at 150 °C, the phases S'', X' and S' co-  
54  
55  
56  
57  
58  
59  
60

1  
2  
3 exist. Pre-ageing at RT promotes X' precipitation at 150 °C (smaller X' peak during  
4 DSC analysis). In alloy 4, formation of X' is even more advanced during the same time  
5  
6  
7  
8 (not shown).  
9

10  
11  
12 **3.2.4. Ageing at 200 °C.** Alloys 1, 2 and 5 were also aged at 200 °C for different times  
13 and examined by DSC (figures 7(a-c)). The curves indicate the presence of GPB zones  
14 after 2 min hold; a certain amount can still form during the scan from the still SSSS.  
15 Figure 7(a) shows that the amount of S'' in alloy 1 decreases progressively in favour of  
16 S' precipitation at ageing times > 10 min; the latter phase is already present after 1 h  
17 hold at 200 °C when the hardness starts its second rise [3]. After 4 hours, the presence  
18 of GPB zones, S'' and S' can be deduced from the subsequent DSC scan; these phases  
19 were actually detected besides clusters in a similar alloy [20]. Dissolution of S'', S' and  
20 S co-existing after 1 day needs about 25 J/g.  
21  
22  
23  
24  
25  
26  
27  
28  
29  
30  
31  
32  
33  
34

35 [Insert figs. 7(a),(b),(c)]

36  
37 Alloy 5 shows a somewhat different behaviour (figure 7(b)). The second  
38 endothermic subpeak increases when prolonging the ageing time at 200 °C from 2 min  
39 to 1 hour; its maximum lies at 270 °C, temperature higher than for alloy 1. This may be  
40 indicative of the presence of an additional phase, probably  $\theta''$  or very small  $\theta'$ . After 4  
41 hours, the DSC curve shows a rather asymmetric precipitation peak. It is proposed that  
42 residual S' formation is preceded by some  $\theta'$  precipitation, as can be observed on aged  
43 Al-4% Cu-0.3% Mg alloys [43]. Diffraction streaks attributed to monolayered GPB  
44 zones by Charaï *et al.* [20] were detected after ageing for 5 min and for 10 h (near peak  
45 hardness) at 200 °C [22,44]. After 15 h hold at 200 °C, a mixture of metastable phases  
46 co-exists and cannot be resolved by DSC (figure 7(b)). In principle, the temperature  
47  
48  
49  
50  
51  
52  
53  
54  
55  
56  
57  
58  
59  
60



1  
2  
3 span of the endothermic effects corresponds to the dissolution of big GPB zones,  $S''$ ,  $\theta''$ ,  
4  
5  
6  $\theta'$  ( $\rightarrow\theta$ ) and  $S'$  ( $\rightarrow S$ ) phases.  
7

8 Curves obtained on the Ag-containing alloy 2 aged at 200 °C (figure 7(c)) confirm  
9  
10 rapid  $X'$  precipitation, as the DSC peak attributable to  $X'$  formation is strongly reduced  
11  
12 after 10 min. A new hardness rise was observed between 3-4 min [3]. At longer ageing  
13  
14 times, DSC analyses start with  $S''$  and  $X'$  dissolution (see curves for 3 and 15 h). The  
15  
16 DSC scan after 1 day ageing indicates  $X'$ ,  $S'$  and  $S$  dissolution.  
17  
18  
19  
20  
21  
22

### 23 3.3. Electron microscopy studies

24  
25 As many observations were already done on the alloys studied (e.g. 15,22,37), only one  
26  
27 heat treatment was examined in order to check the existence of the highly disputed  $S''$   
28  
29 phase. Alloy 1 was quenched and aged at 180 °C for 15 h corresponding to the time  
30  
31 position of the heat flow minimum in figure 2 (curve 1). Figures 8-10 display HRTEM  
32  
33 images and their corresponding Fourier transforms. Clusters are mainly disordered  
34  
35 according to figure 8 which shows no discrete diffraction spots.  
36  
37  
38  
39

40 The precipitate observed on figure 9 is identified as an  $S''$ /GPBII particle  
41  
42 considering that its FFT is identical to those previously published by Charai *et al.* [20]  
43  
44 and Kovarik *et al.* [45]. Based on their HRTEM observations, two structures have been  
45  
46 proposed recently for  $S''$ /GPBII in alloys with Cu:Mg ratios  $>1$  [27] and  $<1$  [45]. Both are  
47  
48 orthorhombic structures coherent with the fcc structure of the matrix but with somewhat  
49  
50 different atom arrangements and compositions. Based on these structures, simulated  
51  
52 HRTEM images and diffraction patterns along one particular orientation match the  
53  
54 observed HRTEM and FFT images.  
55  
56  
57  
58

59 Figure 10 displays the HRTEM image and its FFT of an  $S'$  precipitate, identical  
60  
to those previously published [20].

[Insert figs. 8, 9 and 10]

## 4. Discussion

### 4.1. Formation of clusters and GPB zones.

In this paper, the question of GPB zone formation in an Al-2.5% Cu-1.5% Mg alloy without or with small Ag or Si additions has been re-examined using calorimetric measurements. Considering that the solid solutions are probably short-range ordered (see introduction), it can be expected that this tendency to clustering gets amplified upon quenching and that a metastable phase develops from clusters during ageing. According to figure 1, this phase precipitates at low ageing temperatures via a nucleation and growth controlled process and its heat value amounts to  $-13.5$  J/g. Values of this order accompany the formation of Guinier-Preston zones in many Al-base alloys. In an Al-4% Cu alloy, for instance, formation of GP zones at RT (which contain 25-100 % Cu and whose identification by X-ray or electron diffraction does not constitute any problem) yields about  $-10$  Jg<sup>-1</sup> [46], hence the higher value for the ternary alloy containing less Cu can be explained by the decreased Cu solubility in the presence of Mg and the strong interaction between the Cu and Mg atoms. Therefore it seems reasonable to attribute this peak to the formation of GPB zones, although direct microscopic evidence for their existence in alloys 1–5 aged at temperatures  $< 150$  °C is still lacking due to their extremely small sizes and lack of contrast. This proposition is also supported by Silcock [10] who observed X-ray diffraction effects in single crystals of a similar alloy, Al-3.1% Cu-1.5% Mg aged at RT, and attributed them to the presence of GPB zones. In Al-Mg alloys, GP zones only appear for Mg concentrations above about 10 % [47].

1  
2  
3 The proposed formation of GPB zones during low temperature ageing of Al-Cu-  
4 Mg alloys is in contradiction with recent conclusions of Starink *et al.* [25] drawn from  
5 3D-AP analyses, calorimetric and hardness measurements. The authors propose that  
6 decomposition starts with Cu atom clustering and that Mg co-clustering is responsible  
7 for both the heat flow minimum and rapid hardening.  
8  
9

10  
11  
12  
13  
14  
15 Following Ringer *et al.* [14,15], the cluster sizes observed at 150 °C correspond to  
16 entities of typically 10-50 atoms, hence they contain very few solute atoms. As their  
17 sizes at RT are even smaller and a high concentration of quenched-in vacancies  
18 provides rapid diffusion, formation of clusters is not expected to encounter nucleation  
19 difficulties reflected by a heat flow minimum. Moreover, it may be objected that the  
20 heat values measured on Al-Cu-Mg alloys are too high to correspond to the formation of  
21 clusters which contain only about 10 % solute atoms and many vacancies [23-25].  
22  
23  
24  
25  
26  
27  
28  
29  
30

31  
32 For the S'' phase (or GPBII), Wang and Starink [27] propose a solute  
33 concentration of 37.5%, which seems reasonable as the stable phase contains 50 %  
34 solute atoms.  
35  
36  
37

#### 38 **4.2. Influence of Ag or Si additions**

39  
40  
41 Small Ag additions ranging from 0.4 to 2 % (alloys 2-4) progressively reduce the rate of  
42 GPB zone formation, increasingly with the Ag content. An addition of 0.5 % Si (alloy  
43 5) has a similar but less pronounced effect. These results agree with hardness  
44 measurements when comparing alloys 1 and 2 aged at 30 °C [18] or alloys 1 and 5 aged  
45 at RT [22].  
46  
47  
48  
49  
50  
51  
52

53 A literature survey [48] yields the following binding energy values (in brackets)  
54 between vacancies and the following atoms: Cu (0.20 eV), Si (0.24 eV), Ag (0.27 eV)  
55 and Mg (0.33 eV). Hence Si and Ag atoms also trap vacancies and make the diffusion of  
56 Cu atoms increasingly difficult, thus leading to decreased zone sizes. Applying APFIM  
57  
58  
59  
60

1  
2  
3 to the Ag-bearing alloy 2 aged for 5 min at 150 °C, Ringer *et al.* [15] have detected  
4 Mg-Ag co-clusters besides numerous Mg clusters and Mg-Cu co-clusters. They  
5 consider that Mg-Ag clusters stimulate precipitation of the X' phase. Figure 3 supports  
6 that X' forms the more rapidly the higher is the Ag concentration, hence the cluster  
7 density and the vacancy concentration retained. Pre-ageing at RT does not strongly  
8 influence X' precipitation during DSC heating of alloys 2 and 4 (cf. figures 3 and 4) but  
9 enhances X' formation during isothermal ageing at medium temperatures (curve PA in  
10 figure 6(b)). This may be due to bigger Mg-Ag clusters developed during pre-ageing,  
11 which partly survive.  
12  
13  
14  
15  
16  
17  
18  
19  
20  
21  
22  
23  
24

25 Several effects can be predicted for Si additions to Al-Cu-Mg alloys. Si atoms  
26 may be present in Mg-rich and Si-rich clusters as well as in GPB zones; some zones  
27 characteristic of Al-Mg-Si alloys may also appear. EDS spectra of Hutchinson and  
28 Ringer [22] show that clusters called GPB zones contain Cu, Mg, Si and Al.  
29 Furthermore, it has to be taken into account that only a small amount of Si (up to about  
30 0.1%) is soluble at 520 °C in the present ternary alloy [22]; the excess Si is bound in the  
31 form of Mg<sub>2</sub>Si, hence it decreases the soluble Mg content and the as-quenched hardness  
32 value. The alloy shifts progressively from the ( $\alpha + S$ ) into the ( $\alpha + S + \theta$ ) phase field, as  
33 described by Hutchinson and Ringer [22]. Hence the precipitation behaviour will  
34 depend on the Si content:  
35  
36  
37  
38  
39  
40  
41  
42  
43  
44  
45  
46  
47  
48

49 - According to Smith *et al.* [38], a Si addition of 0.1 % slightly enhances S'  
50 formation. Nucleation may be easier in the presence of soluble Si which interacts with  
51 Mg and vacancies and decreases the shear strain energy [49] and the critical nucleus  
52 size for S' precipitation [50]. Smith *et al.* related the enhancement to earlier zone  
53 dissolution which is indeed necessary before S' precipitation and contradicts the  
54 commonly accepted continuous sequence SSSS  $\rightarrow$  GPB zones  $\rightarrow$  S''  $\rightarrow$  S'  $\rightarrow$  S. The  
55  
56  
57  
58  
59  
60

1  
2  
3 present DSC curves indicate that direct transformation of GPB zones and  $S''$  into  $S'$  is of  
4 little significance at a heating rate of  $20 \text{ Kmin}^{-1}$ . This also applies to binary Al-Cu  
5  
6  
7  
8 alloys: during heating at  $20 \text{ Kmin}^{-1}$ , all GP zones dissolve before precipitation of  $\theta'$ ; at  
9  
10 lower rates, however, reversion is only partial [51,52].  
11

12  
13 - When the Si content exceeds the solubility limit, as in alloy 5,  $\text{Mg}_2\text{Si}$  particles  
14 are present after quenching and  $S'$  formation is delayed with respect to the ternary alloy,  
15 especially after ageing at RT (figure 2). Slower  $S'$  precipitation was also found in earlier  
16 DSC measurements [36] and in mechanical property and TEM studies of Wilson *et al.*  
17 [35]. They have attributed the observed refined size distribution of the  $S'$  particles to a  
18 more homogeneous nucleation process related to the decreased density of dislocation  
19 loops and helices in the presence of Si. The present DSC curves indicate some  $S'$  size  
20 refinement, the exothermic peak around  $300 \text{ }^\circ\text{C}$  being sharper for alloy 5 than for alloy  
21 1 (figure 3).  
22  
23  
24  
25  
26  
27  
28  
29  
30  
31  
32  
33  
34  
35  
36  
37

#### 38 **4.3. Influence of pre-ageing at RT on $S'$ precipitation**

39 During continuous heating, the shape and temperature range of the main exothermic  
40 effects observed on alloy 1 change when RT ageing is carried out after quenching. The  
41 peaks become sharper indicating  $S'$  size refinement; their initial, peak and end  
42 temperatures shift progressively to lower values with increasing ageing time (cf. curve  
43 1 in figure 3, curves a, b and c in figure 5 and curve 1 in figure 4). On the contrary, pre-  
44 ageing at RT has no significant influence on  $S'$  precipitation during heating of alloy 5  
45 (cf. curves 5 in figure 3 and 4). This is also true in the case of a reverted alloy 1;  
46 samples aged after reversion have  $S'$  peaks similar to those of curve 4 in figure 5.  
47  
48  
49  
50  
51  
52  
53  
54  
55  
56  
57  
58

59 The changes observed on alloy 1 can be explained by an easier homogeneous  
60 nucleation (the main process accompanied by heat flow minima in figure 2) resulting

1  
2  
3 from a higher density of clusters of overcritical size and/or by easier heterogeneous  
4 nucleation due to an increased defect density. In fact, the density and size of dislocation  
5 loops become higher when ageing alloy 1 at RT (Hutchinson and Ringer [22]), whereas  
6 loop formation is expected to be negligible after reversion due to vacancy loss at 230  
7 °C. Growth of helices was observed in the Si-bearing alloy 5 during prolonged natural  
8 ageing but loops were not seen [22]. It seems that in a quenched ternary alloy, RT  
9 ageing favours mainly heterogeneous precipitation on dislocation loops, in agreement  
10 with Ber and Davydov [53]. Dislocations introduced by cold working in a quenched  
11 ternary alloy also strongly enhance S' precipitation upon heating and assure a finer size  
12 distribution which improves the mechanical properties of the alloy [29].  
13  
14  
15  
16  
17  
18  
19  
20  
21  
22  
23  
24  
25  
26  
27  
28

#### 29 **4.4. First and second hardening stages**

30  
31 It was proposed by Charai *et al.* [20] that in quenched Al-2%Cu-1.3%Mg alloys having  
32 a Mg:Cu atomic ratio of 1.6, GPB zones develop from very small Cu-rich clusters  
33 during the first minutes of ageing, whereas Mg-rich clusters containing excess vacancies  
34 absorb Cu atoms and become effective nuclei only at medium temperatures. In fact, the  
35 as-quenched hardness (AQ) values of Al-2.5% Cu alloys with Mg additions varying  
36 from 0.5 to 2%, are increasing with the Mg content, whereas the net hardness rise  
37 during the first hardening stage is similar except for the alloy containing only 0.5% Mg,  
38 hence with a Mg:Cu atomic ratio < 1 (Vietz and Polmear [3]). Also during the second  
39 stage of hardening in semi-logarithmic presentation, the net increase is rather  
40 independent of the Mg concentration in the range 150–200 °C, yet its onset is  
41 progressively delayed with increasing Mg content. In fact, Mg atoms are expected to  
42 inhibit Cu atom diffusion which seems to be the rate controlling step.  
43  
44  
45  
46  
47  
48  
49  
50  
51  
52  
53  
54  
55  
56  
57  
58  
59  
60

1  
2  
3 The important heat values measured on alloys lying in the ( $\alpha + S$ ) region of the  
4 ternary phase diagram depend primarily on the Cu content of the alloy. This supports  
5 the idea that GPB zones are responsible for the **first hardness stage**. The initial  
6 hardness increase at RT in an Al-4.4% Cu-1.7% Mg alloy has also been assigned to the  
7 formation of GP and GPB zones [54]. Clusters which contain much less solute atoms,  
8 are expected to contribute already to the AQ hardness level via the cluster hardening  
9 mechanism first proposed by Ringer *et al.* [15,26]. Other mechanisms may also be  
10 involved such as SS hardening, modulus hardening [25], dislocation loop hardening  
11 [17], solute atom - dislocation interactions [8] which favour subsequent heterogeneous  
12 nucleation of S' and S.  
13  
14  
15  
16  
17  
18  
19  
20  
21  
22  
23  
24  
25  
26

27 The sizes of GPB zones (and probably of some Si-modified GPB zones in Si-  
28 bearing alloys) decrease when adding Si, and even more when adding Ag to the ternary  
29 alloy. This zone refinement may be mainly responsible for the fact that a higher net  
30 hardness increase at 150 °C (difference between value obtained after 2 min ageing and  
31 AQ value) is achieved when adding Ag (Vietz and Polmear [3]) than when adding Si  
32 [39], considering equivalent Cu and Mg concentrations in these alloys. It has also been  
33 shown [18] that the hardness of alloy 2 surpasses that of alloy 1 for long ageing times at  
34 30 °C. At 200 °C, however, there is an exceptionally high increase when adding Si; it  
35 can be attributed to the formation of additional phases typical for Al-Cu alloys, namely  
36  $\theta''$  via GP zones and  $\theta'$ , as alloy 5 lies at the border of the ( $\alpha + \theta + S$ ) field of the phase  
37 diagram section at 190 °C [22]. In fact, GP zones were found in Al-1.5 %Cu-0.75 %Mg  
38 alloys containing >0.3 % Si [55]. The presence of  $\theta'$  was observed by Gupta *et al.* [56]  
39 at 190 °C (>0.3 % Si); Hutchinson and Ringer [22] found  $\theta$  and  $\sigma(\text{Al}_5\text{Cu}_6\text{Mg}_2)$  in  
40 overaged alloy 5 ( $\geq 20$  h at 200 °C). Hence the asymmetry in the exothermic peaks in  
41 figure 2 (curve 5 at 180 °C) and figure 7(b) (4h at 200 °C) can be attributed to (further)  
42  
43  
44  
45  
46  
47  
48  
49  
50  
51  
52  
53  
54  
55  
56  
57  
58  
59  
60

1  
2  
3  $\theta'$  and  $S'$  formation. The  $\theta'$  phase is expected to precipitate earlier than the  $S'$  phase, as  
4  
5  
6 the less stable GP zones dissolve earlier [43].  
7

8  
9  
10 A comparison of the hardness (Vietz and Polmear [3]) and DSC measurements  
11 (figures 6(a) and 7(a)) shows that during the **second hardness rise** at 150 °C (>1 day)  
12 and 200 °C (>1 h), the proportion of GPB zones and  $S''$  diminishes and that of  $S'$   
13  
14 increases in the ternary alloy. Hence this stage can be related to fine  $S'$  particles which  
15  
16 precipitate probably at the sites of clusters, as shown by HRTEM [22,30]. The necessary  
17  
18 Cu atoms are provided by the progressive dissolution of less stable phases and the  
19  
20 decreased solute solubility in the presence of more stable phases, which increases the  
21  
22 fraction precipitated and the corresponding heat value.  
23  
24  
25  
26

27  
28 In the Ag containing alloys 2-4, the second hardening stage sets in rapidly at  
29  
30 medium temperatures. According to hardness measurements on alloy 2 aged at 150 °C,  
31  
32 its start falls between 1 h [3] and 10 h [57]; these largely varying times may be due to  
33  
34 difficult subjective appreciation and different experimental conditions. DSC scans  
35  
36 indicate already  $S''$  and  $X'$  formation in this time range (figure 6(b)). The precipitation  
37  
38 of  $X'$  continues between 1 and 4 days, whereas GPB zones and  $S''$  dissolve  
39  
40 progressively and some  $S'$  appears. Hence the second hardness rise may be attributed  
41  
42 mainly to the precipitation of the  $X'$  phase, as proposed by Ringer *et al.* [15], and  
43  
44 supports the proposition of its initial coherency with the matrix. At peak hardness  
45  
46 reached between 5 [3] and 20 days,  $X'$  is probably semi-coherent (Ferragut *et al.* [57]).  
47  
48  
49  
50

51  
52 When alloy 2 is aged at 200 °C, a second hardness rise becomes observable in  
53  
54 semi-logarithmic presentation after 3-4 min [3]. According to figure 7(c), there is  
55  
56 notable precipitation of the  $X'$  phase between 2 and 10 min,  $S''$  being also present and  
57  
58 dissolving in favour of  $S'$  at longer ageing times. At maximum hardness (about 3 h), the  
59  
60



1  
2  
3 phases  $S''$ ,  $X'$  and  $S'$  co-exist, as a subsequent DSC scan starts with  $S''$  and  $X'$   
4  
5 dissolution before precipitation of residual  $S'$ .  
6  
7  
8  
9

## 10 5. Conclusions

11  
12 Calorimetric measurements at constant temperatures and during heating at 20  
13  $K.min^{-1}$  provided the following information about the effects of 0.4 to 2% Ag or 0.5%  
14  
15 Si additions to an Al-2.5 mass% Cu-1.5 mass% Mg alloy:  
16  
17

- 18 1 The precipitation of GPB zones obeys a well visible nucleation and growth  
19 controlled process at low temperatures; its rate is reduced with respect to the  
20 ternary alloy due to the vacancy-trapping effect of soluble Si and, even more, of  
21 Ag atoms. This results in zone refinement and hardness increases.  
22  
23
- 24 2 A Si addition of 0.5% induces  $\theta'$  prior to  $S'$  precipitation at medium temperatures.  
25  
26
- 27 3 In the Ag-containing alloys, an additional phase,  $X'$ , appears before  $S'$ . It forms  
28 earlier when the Ag addition (hence the density of Mg-Ag clusters) is increased.  
29  
30
- 31 4 Pre-ageing at RT enhances  $S'$  formation in the ternary alloy and causes a narrower  
32 size distribution; in an alloy containing 0.5% Si, it retards isothermal  $\theta'$  and  $S'$   
33 formation; in the Ag-containing alloys, it promotes isothermal  $X'$  formation.  
34  
35
- 36 5 Correspondence between DSC curves and existing hardness data support the  
37 original interpretation, i.e. the first hardening stage results from the formation of  
38 GPB zones which transform into the  $S''$  phase (the existence of which was again  
39 proven by HRTEM). During the second hardening stage in logarithmic time scale,  
40  $S'$  particles nucleate after incomplete reversion of GPB zones and  $S''$ , and increase  
41 the volume fraction precipitated.  
42  
43
- 44 6 In the Ag-containing alloys, the second hardening stage sets in much earlier than  
45 in the ternary alloy and is related mainly to the precipitation of  $X'$ .  
46  
47  
48  
49  
50  
51  
52  
53  
54  
55  
56  
57  
58  
59  
60

1  
2  
3 7 The very high hardness increases in the Si-containing alloy can be attributed to the  
4  
5 formation of additional phases typical for binary Al-Cu alloys.  
6  
7  
8  
9

#### 10 Acknowledgements

11  
12 The authors are greatly indebted to Dr. W. Saikaly who carried out the high resolution  
13 electron microscopic studies at the Centre Pluridisciplinaire de Microscopie  
14 électronique et de Microanalyse. They also thank Prof. I.J. Polmear of Monash  
15 University (Australia) for the alloy supply and many fruitful discussions.  
16  
17  
18  
19  
20  
21  
22  
23  
24  
25  
26  
27  
28  
29  
30  
31  
32  
33  
34  
35  
36  
37  
38  
39  
40  
41  
42  
43  
44  
45  
46  
47  
48  
49  
50  
51  
52  
53  
54  
55  
56  
57  
58  
59  
60

## References

- [ 1] G.B. Brook, *Precipitation in Metals*, Special Report n° 3 (Fulmer Research Institute, Stoke Poges, UK, 1963).
- [ 2] H.K. Hardy, *J. Inst. Met.* **83** 17 (1954-55).
- [ 3] J.T. Vietz and I.J. Polmear, *J. Inst. Met.* **94** 410 (1966).
- [ 4] P. Vigier, A.-M. Zahra-Kubik, M. Denoux, J.P. Brisset and M. Wintenberger, *Mém. Sci. Rev. Mét.* **69** 51 (1972).
- [ 5] E. Matsubara and J.B. Cohen, *Acta metall.* **31** 2129 (1983).
- [ 6] P. Chartrand and A.D. Pelton, *J. Phase Equil.* **15** 591 (1994).
- [ 7] B.-P. Huang and Z.-Q. Zheng, *Acta mater.* **46** 4381 (1998).
- [ 8] L. Reich, S.P. Ringer, and K. Hono, *Phil. Mag. Lett.* **79** 639 (1999).
- [ 9] S. Hirose, T. Sato, A. Kamio and H.M. Flower, *Acta mater.* **48** 1797 (2000).
- [10] J.M. Silcock, *J. Inst. Met.* **89** 203 (1960-61).
- [11] A.-M. Zahra and C.Y. Zahra, *Phil. Mag. Lett.* **82** 9 (2002).
- [12] B. Verlinden and A.-M. Zahra, *Mater. Sci. Forum* **426-432** 423 (2003).
- [13] S.P. Ringer, K. Hono, I.J. Polmear and T. Sakurai, *Appl. Surf. Sci.* **94-95** 253 (1996).
- [14] S.P. Ringer, K. Hono, T. Sakurai and I.J. Polmear, *Scripta mater.* **36** 517 (1997).
- [15] S.P. Ringer, T. Sakurai and I.J. Polmear, *Acta mater.* **45** 3731 (1997).
- [16] K. Raviprasad, C.R. Hutchinson, T. Sakurai and S.P. Ringer, *Acta mater.* **51** 5037 (2003).
- [17] S. Kumai, M. Okutsu, N. Yoneyama and T. Sato, *J. Jpn. Inst. Light Met.* **52** 465 (2002).
- [18] I.J. Polmear, *Trans. Metall. Soc. AIME* **230** 1331 (1964).
- [19] M.J. Starink and A.-M. Zahra, *Thermochim. Acta* **298** 179 (1997).

- 1  
2  
3 [20] A. Charai, T. Walther, C. Alfonso, A.-M. Zahra and C.Y. Zahra, *Acta mater.* **48**  
4  
5 2751 (2000).  
6  
7  
8 [21] Y.A. Bagaryatskii, *Dokl. Akad. NAUK SSSR* **87** 559 (1952).  
9  
10 [22] C.R. Hutchinson and S.P. Ringer, *Metall. Mater. Trans.* **31A** 2721 (2000).  
11  
12 [23] N. Gao, L. Davin, S. Wang, A. Cerezo and M.J. Starink, *Mater. Sci. Forum* **396-**  
13  
14 **402** 923 (2002).  
15  
16 [24] A.-M. Zahra, C.Y. Zahra, C. Alfonso and A. Charai, *Scripta Mater.* **39** 1553  
17  
18 (1998).  
19  
20 [25] M.J. Starink, N. Gao, L. Davin, J. Yan and A. Cerezo, *Phil.Mag.* **85** 1395 (2005).  
21  
22 [26] S.P. Ringer, S.K. Caraher and I.J. Polmear, *Scripta mater.* **39** 1559 (1998).  
23  
24 [27] S.C. Wang and M.J. Starink, *Mater. Sci. Eng.* **A386** 156 (2004).  
25  
26 [28] H.-C. Shih, N.-J. Ho and J.C. Huang, *Metall. Mater.Trans.* **27A** 2479 (1996).  
27  
28 [29] A.-M. Zahra and C.Y. Zahra, *J. Therm. Anal.* **36** 1465 (1990).  
29  
30 [30] V. Radmilovic, G. Thomas, G.J. Shiflet and E.A. Starke, *Scripta metall.* **23** 1141  
31  
32 (1989).  
33  
34 [31] G. Riontino and A. Zanada, *Mater. Lett.* **37** 241 (1998).  
35  
36 [32] V. Radmilovic, R. Kilaas, U. Dahmen and G.J. Shiflet, *Acta mater.* **47** 3987  
37  
38 (1999).  
39  
40 [33] C. Wolverton, *Acta mater.* **49** 3129 (2001).  
41  
42 [34] L.F. Mondolfo, 1976, *Aluminium Alloys : Structure and Properties* (Butterworths,  
43  
44 London, 1976).  
45  
46 [35] R.N. Wilson, D.M. Moore and P.J.E. Forsythe, *J. Inst. Met.* **95** 177 (1967).  
47  
48 [36] H. Kee Cho and K. Hirano, paper presented at the 5<sup>th</sup> Internat. Conf. Therm. Anal.,  
49  
50  
51  
52  
53  
54  
55  
56  
57  
58  
59  
60  
Kyoto, Japan (1977).

- 1  
2  
3 [37] H.D. Chopra, L.J. Liu, B.C. Muddle and I.J. Polmear, *Phil. Mag. Lett.* **71** 319  
4  
5 (1995).  
6  
7  
8 [38] G.W. Smith, W.J. Baxter and R.K. Mishra, *J. Mater. Sci.* **35** 3871 (2000).  
9  
10 [39] S.P. Ringer, I.J. Polmear and T. Sakurai, *Mater. Sci. Eng.* **A217-218** 273 (1996).  
11  
12 [40] L. Reich, K. Süvegh, J. Lendvai and A. Vertes, *Phil. Mag. Lett.* **81** 145 (2000).  
13  
14 [41] A.-M. Zahra and M. Laffitte, *Scripta metall.* **8** 165 (1974).  
15  
16 [42] C.Y. Zahra and A.-M. Zahra, *Thermochim. Acta* **276** 161 (1996).  
17  
18 [43] A.-M. Zahra, C.Y. Zahra, K. Raviprasad and I.J. Polmear, *Phil. Mag.* **84** 2521  
19  
20 (2004).  
21  
22 [44] C.R. Hutchinson, K. Raviprasad and S.P. Ringer, in *Proc. Internat. Conf. Solid-*  
23  
24 *Solid Phase Transformations '99 (JIMIC-3)*, edited by M. Koiwa, K. Otsuka and  
25  
26 T. Miyazaki (*Jpn. Inst. Met.*, 1999), p. 169.  
27  
28 [45] L. Kovarik, P.I. Gouma, C. Kisielowski, S.A. Court and M.J. Mills, *Acta Mater.*  
29  
30 **52** 2509 (2004).  
31  
32 [46] A. Zahra, M. Laffitte, P. Vigier and M. Wintenberger, *Mém. Sci. Rev. Mét.* **74** 561  
33  
34 (1977).  
35  
36 [47] M.J. Starink and A.-M. Zahra, *Phil. Mag.* **A76** 701 (1997).  
37  
38 [48] H. Löffler, *Structure and Structure Development of Al-Zn Alloys* (Akademie-  
39  
40 Verlag, Berlin, Germany, 1995), p. 56.  
41  
42 [49] J.F. Nie, H.I. Aronson and B.C. Muddle, in *Proc. Internat. Conf. Solid-Solid*  
43  
44 *Phase Transformations '99 (JIMIC-3)*, edited by M. Koiwa, K. Otsuka and T.  
45  
46 Miyazaki (*Jpn. Inst. Met.*, 1999), p. 157.  
47  
48 [50] F. Soisson and G. Martin, *Phys. Rev.* **B62** 203 (2000).  
49  
50 [51] A.-M. Zahra, M. Laffitte, P. Vigier and M. Wintenberger, *C. R. Acad. Sci.* **C277**  
51  
52 923 (1973).  
53  
54  
55  
56  
57  
58  
59  
60

- 1  
2  
3 [52] A. Zahra-Kubik, M. Laffitte, P. Vigier and M. Wintenberger, Aluminium, **52** 357  
4  
5 (1976).  
6  
7  
8 [53] L.B. Ber and V.G. Davydov, Mater. Sci. Forum **396-402** 983 (2002).  
9  
10 [54] S. Abis, M. Massazza, P. Mengucci and G. Riontino, Scripta mater. **45** 685 (2001).  
11  
12 [55] A.K. Jena, A.K. Gupta and M.C. Chaturvedi, Metall. Trans. **24A** 2181 (1993).  
13  
14 [56] A.K. Gupta, M.C. Chaturvedi and A.K. Jena, Mater. Sci. Technol. **5** 52 (1989).  
15  
16 [57] R. Ferragut, A. Somoza, A. Dupasquier and I.J. Polmear, Mater. Sci. Forum **396-**  
17  
18 **402** 777 (2002).  
19  
20  
21  
22  
23  
24  
25  
26  
27  
28  
29  
30  
31  
32  
33  
34  
35  
36  
37  
38  
39  
40  
41  
42  
43  
44  
45  
46  
47  
48  
49  
50  
51  
52  
53  
54  
55  
56  
57  
58  
59  
60

## Figure Captions

Fig. 1: Isothermal calorimetry: heat flows of pure aluminium and of alloys 1, 2, 3 and 5 aged in the calorimeter at 30 °C.

Fig. 2: Isothermal calorimetry: heat flows recorded during ageing at 180 °C on alloy 1 after water quenching (curve 1), followed by ageing for 7 days at RT (curve 1a), or 4 days at 100°C (1b) and on alloy 5 after water quenching (curve 5) and followed by ageing for 7 days at RT (curve 5a).

Fig. 3: DSC at 20Kmin<sup>-1</sup> on alloys 1, 2, 4 and 5 after water quenching.

Fig. 4: DSC at 20Kmin<sup>-1</sup> on alloys 1, 2, 4 and 5 after water quenching and long room temperature ageing (9 months for alloys 1, 2, 4 and 14 months for alloy 5).

Fig. 5: DSC at 20Kmin<sup>-1</sup> on alloy 1 after water quenching and ageing at RT for 3 hours (a), 7 hours (b), 1 day (c) or after water quenching and ageing for 4 minutes at 230°C (d).

Fig. 6: DSC at 20Kmin<sup>-1</sup> on alloy 1 (a) and alloy 2 (b) after water quenching and ageing at 150 °C for times indicated on the figures. The response of samples pre-aged at RT (8 days for alloy 1, 2 months for alloy 2) after water quenching and aged at 150 °C for 1 day is also displayed (curves PA).

Fig. 7: DSC at 20Kmin<sup>-1</sup> on alloy 1 (a), alloy 5 (b) and alloy 2 (c) after water quenching and ageing at 200 °C for times indicated on the figures.

Fig. 8: HRTEM image (a) and its Fourier transform (b) of a cluster observed in alloy 1 after water quenching and ageing for 15h at 180°C.

Fig. 9: HRTEM image (a) and its Fourier transform (b) confirming the presence of the S'' phase in alloy 1 after water quenching and ageing for 15h at 180°C.

Fig. 10: HRTEM image (a) and its Fourier transform (b) of a precipitate of the S' phase observed in alloy 1 after water quenching and ageing for 15h at 180°C.

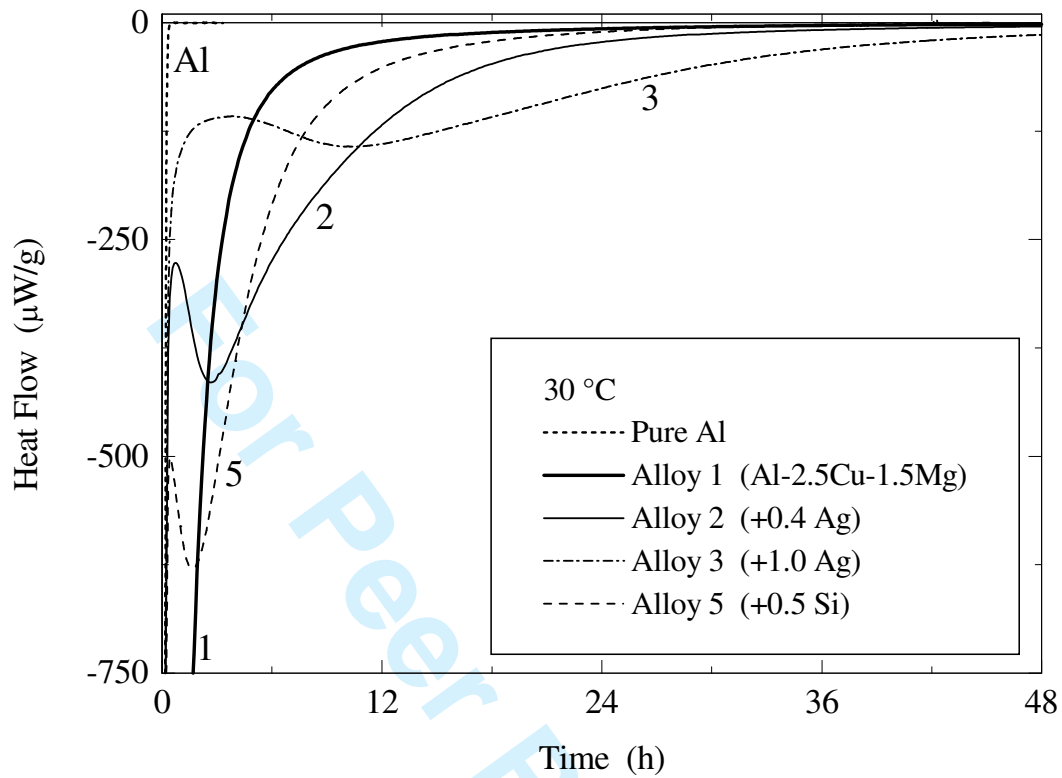


Figure 1: Isothermal calorimetry: heat flows of pure aluminium and of alloys 1, 2, 3 and 5 aged in the calorimeter at 30 °C.



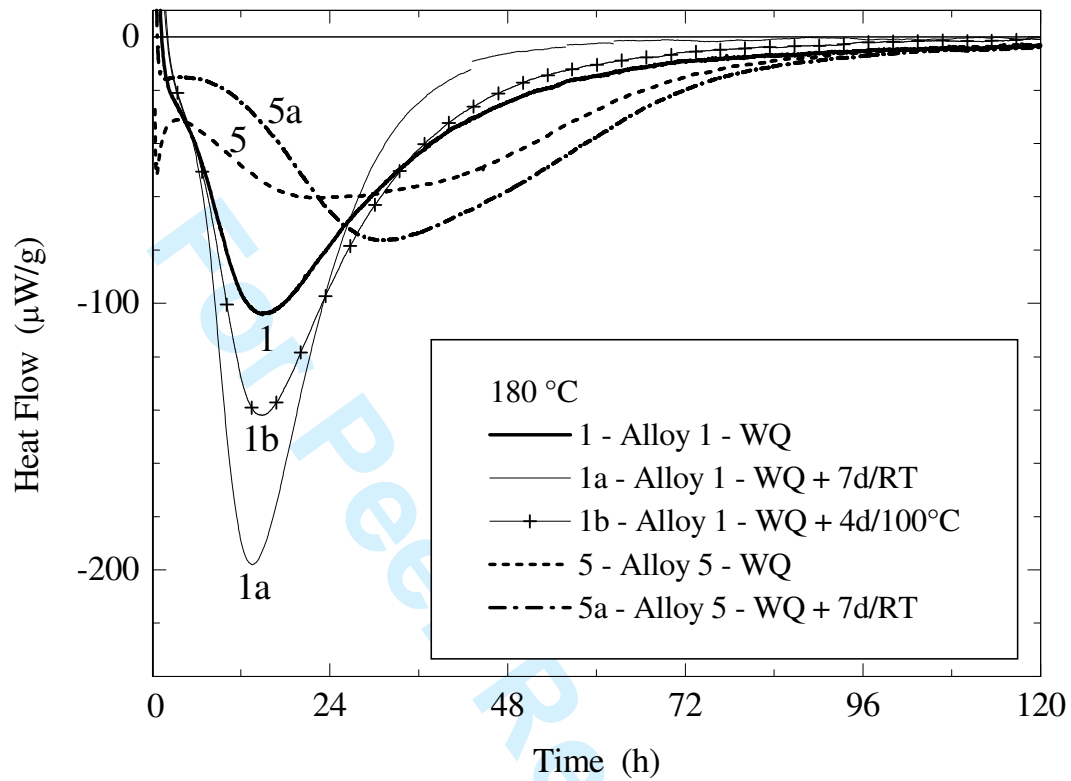


Figure 2: Isothermal calorimetry: heat flows recorded during ageing at 180 °C on alloy 1 after water quenching (curve 1), followed by ageing for 7 days at RT (curve 1a), or 4 days at 100°C (1b) and on alloy 5 after water quenching (curve 5) and followed by ageing for 7 days at RT (curve 5a).

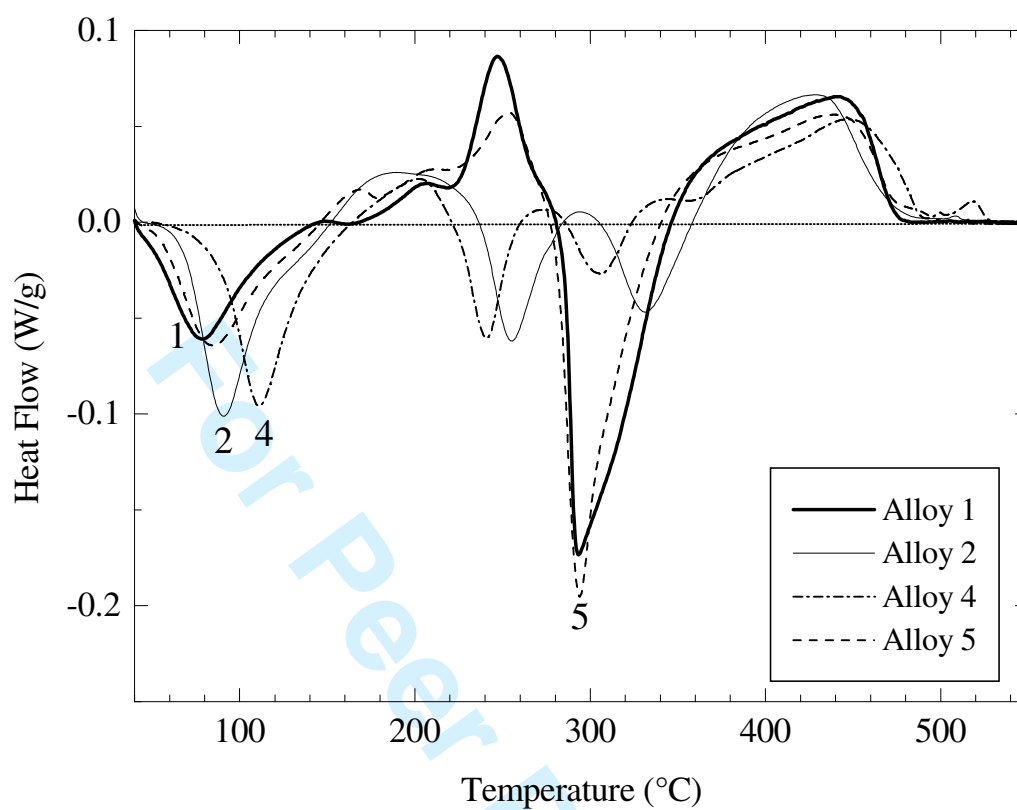


Figure 3: DSC at  $20\text{Kmin}^{-1}$  on alloys 1, 2, 4 and 5 after water quenching.

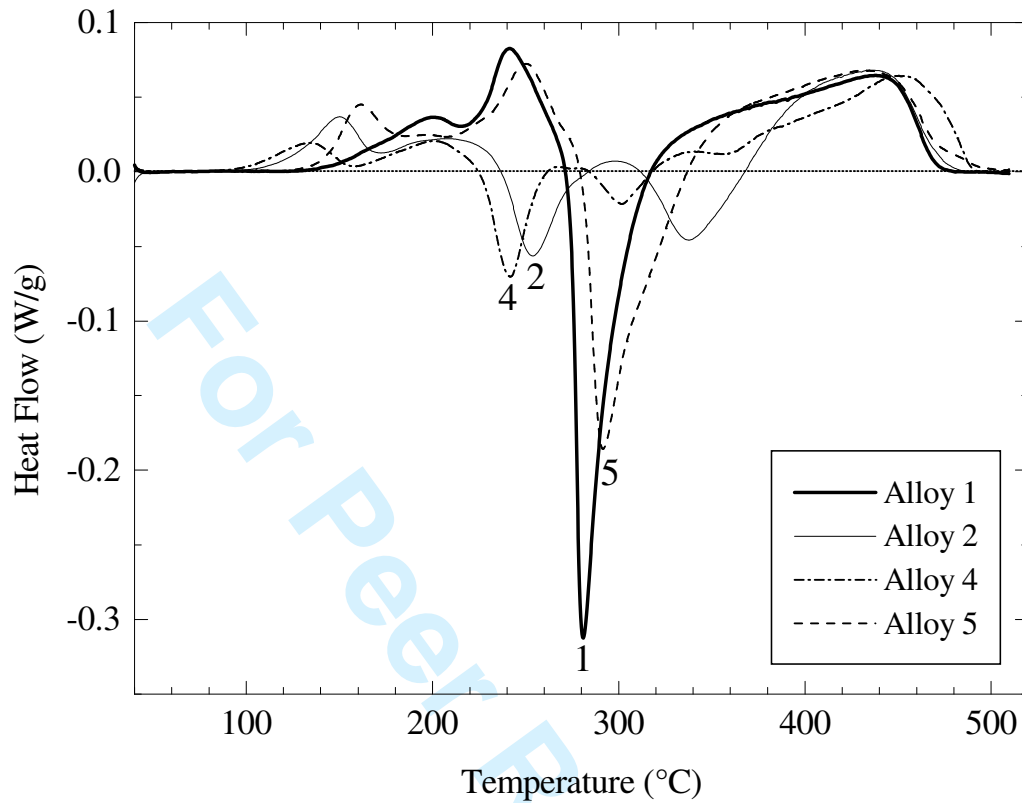


Figure 4: DSC at  $20\text{Kmin}^{-1}$  on alloys 1, 2, 4 and 5 after water quenching and long room temperature ageing (9 months for alloys 1, 2, 4 and 14 months for alloy 5).

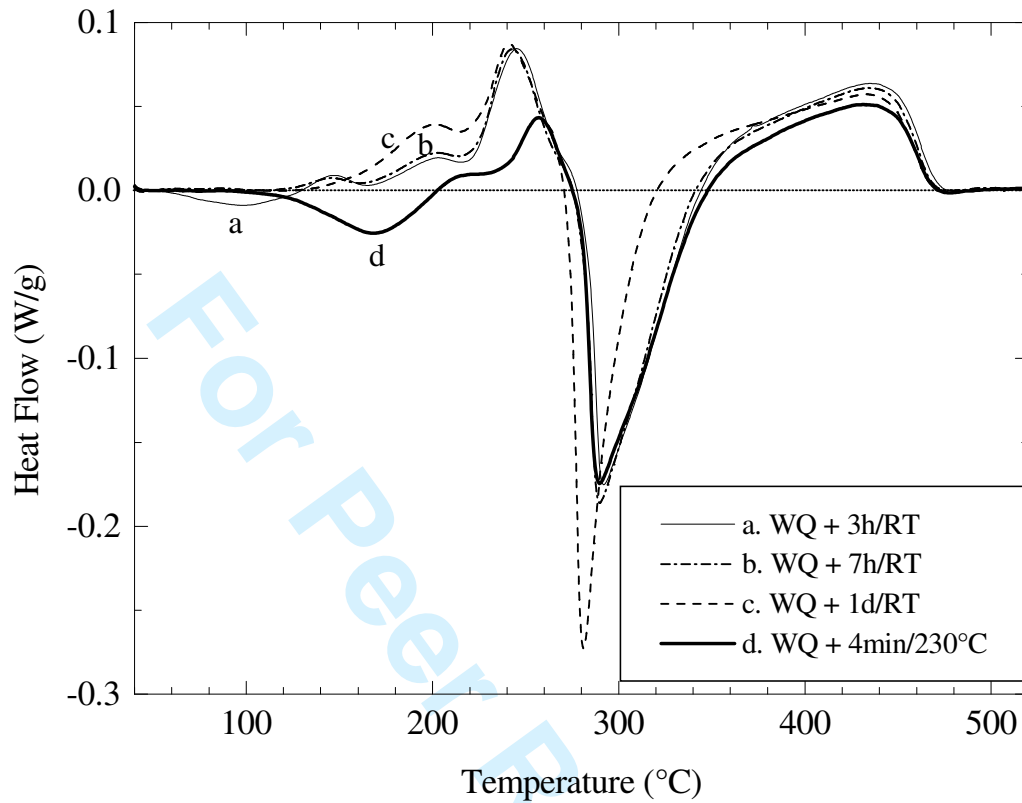


Figure 5: DSC at  $20\text{Kmin}^{-1}$  on alloy 1 after water quenching and ageing at RT for 3 hours (a), 7 hours (b), 1 day (c) or after water quenching and ageing for 4 minutes at  $230^\circ\text{C}$  (d).

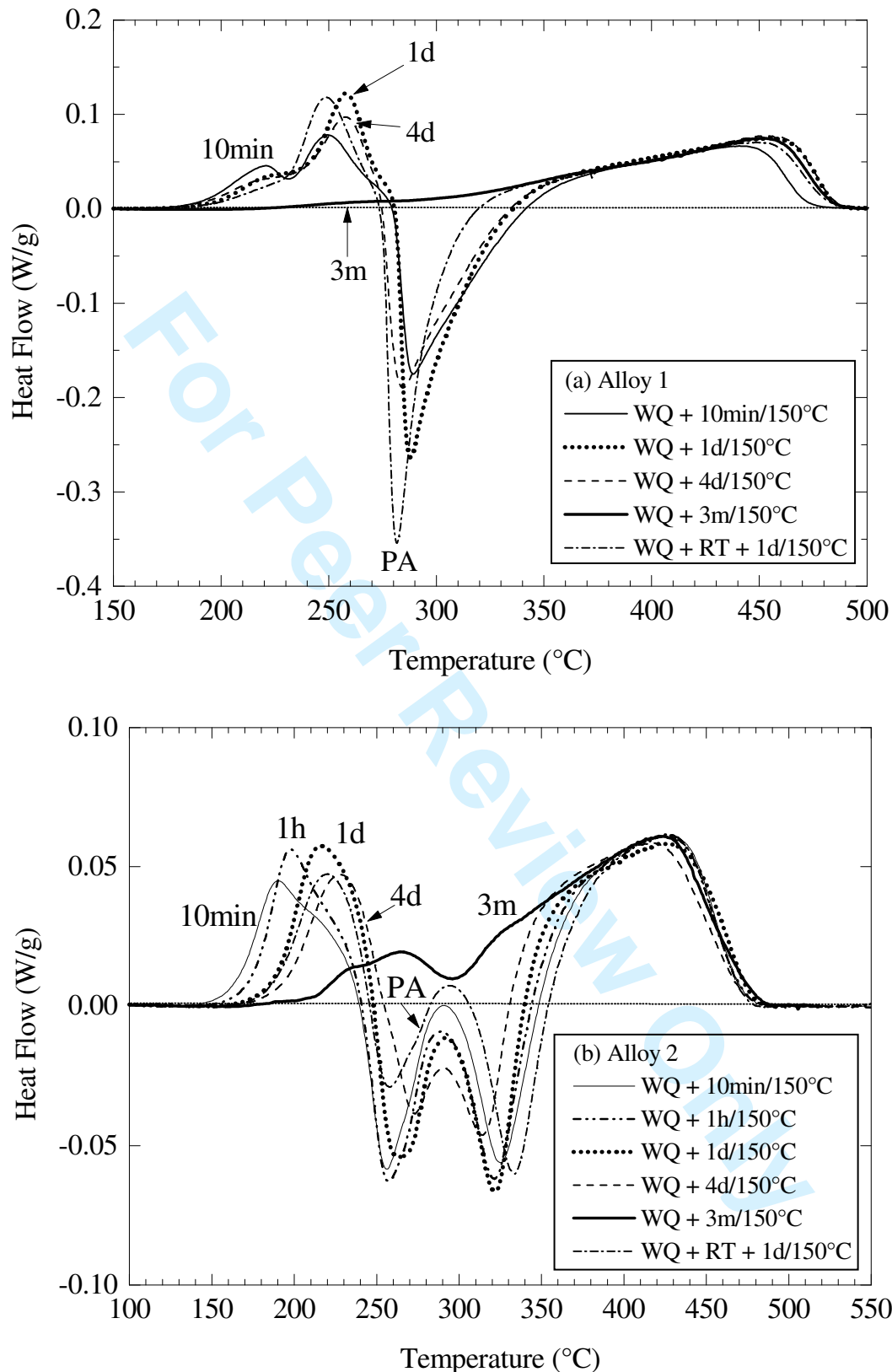
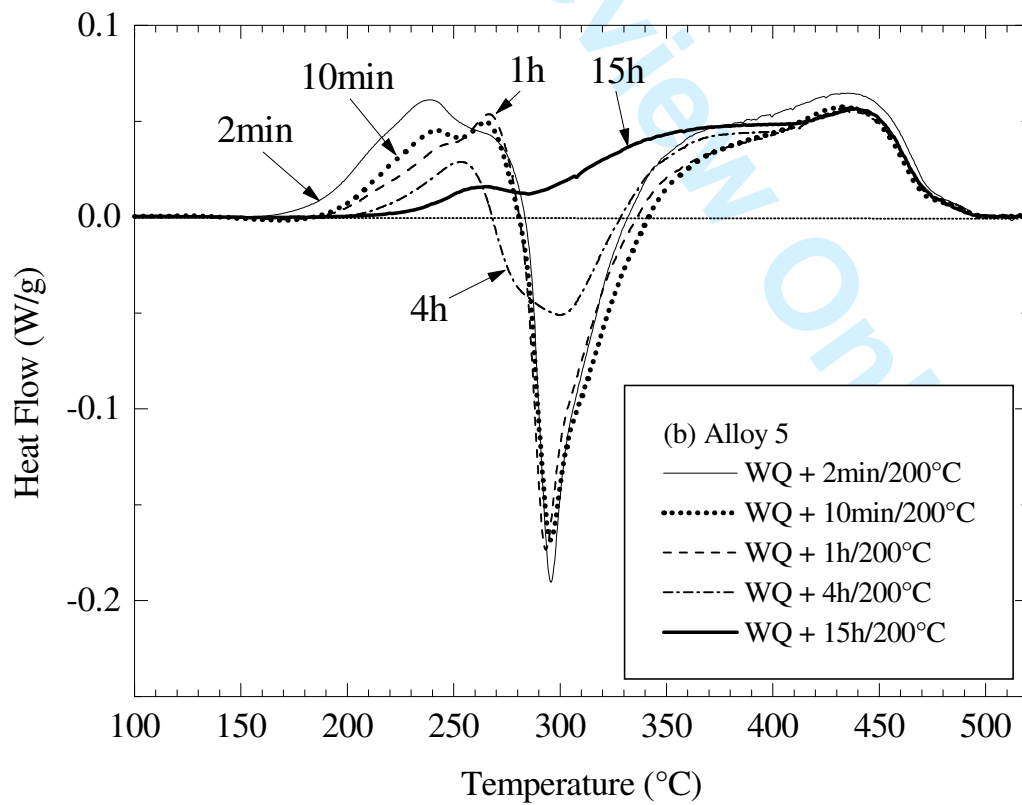
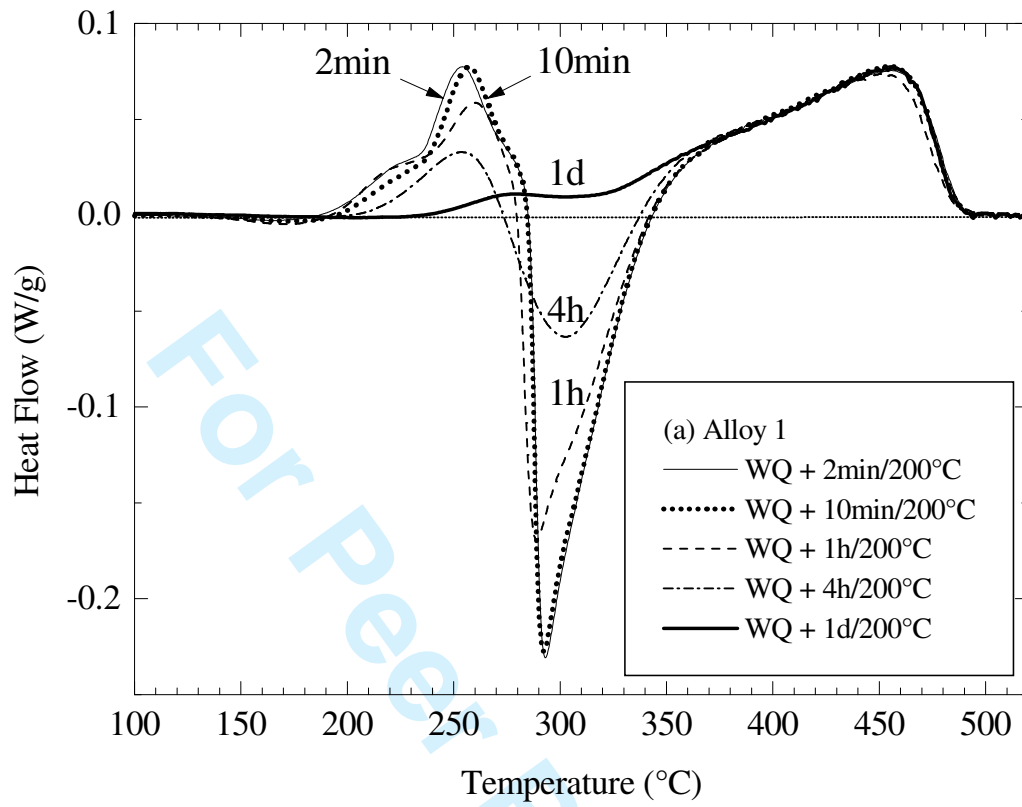


Figure 6: DSC at  $20\text{Kmin}^{-1}$  on alloy 1 (a) and alloy 2 (b) after water quenching and ageing at  $150^\circ\text{C}$  for times indicated on the figures. The response of samples pre-aged at RT (8 days for alloy 1, 2 months for alloy 2) after water quenching and aged at  $150^\circ\text{C}$  for 1 day is also displayed (curves PA).



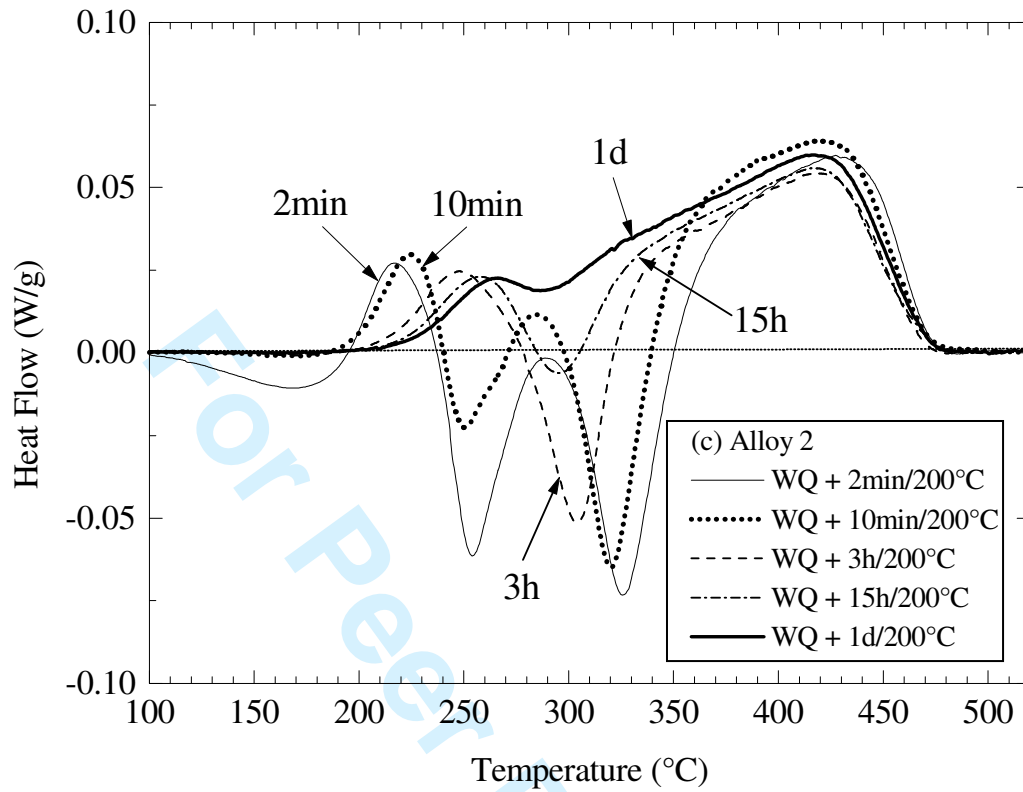


Figure 7: DSC at  $20\text{Kmin}^{-1}$  on alloy 1 (a), alloy 5 (b) and alloy 2 (c) after water quenching and ageing at  $200\text{ }^\circ\text{C}$  for times indicated on the figures.

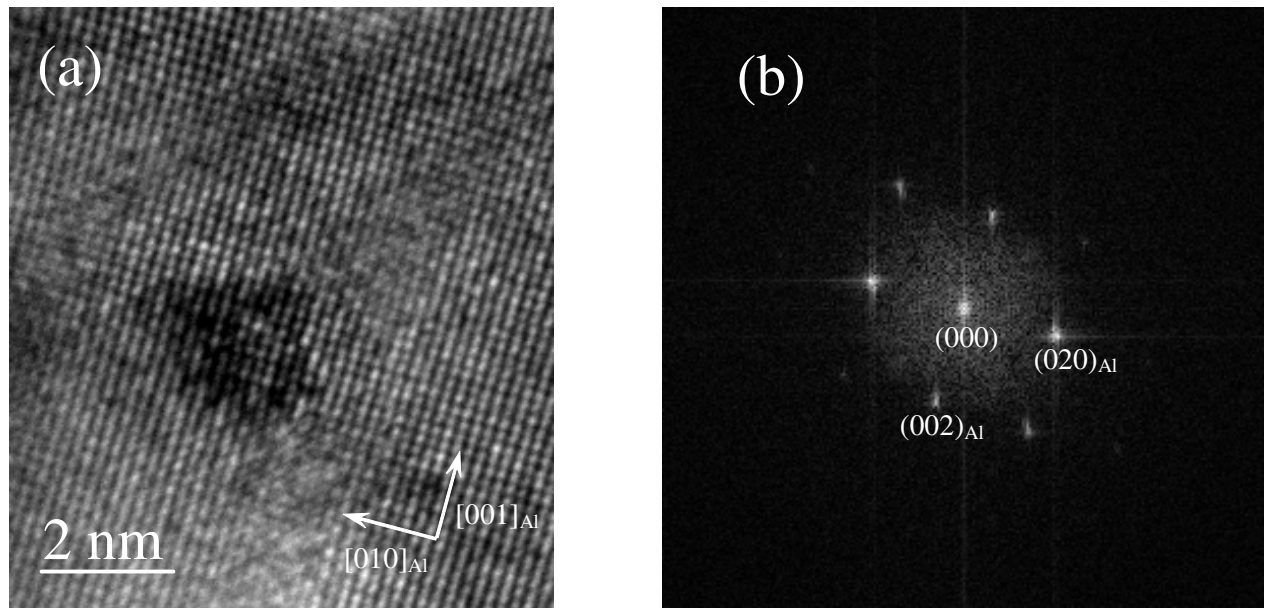


Figure 8: HRTEM image (a) and its Fourier transform (b) of a cluster observed in alloy 1 after water quenching and ageing for 15h at 180°C.



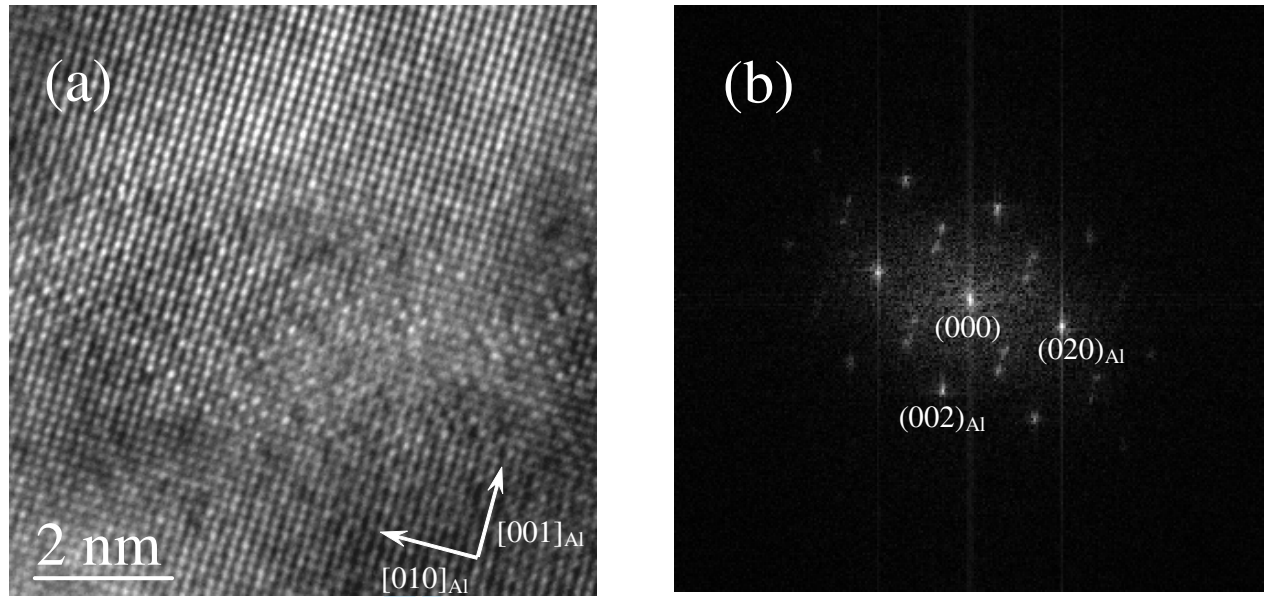


Figure 9: HRTEM image (a) and its Fourier transform (b) confirming the presence of the S'' phase in alloy 1 after water quenching and ageing for 15h at 180°C.

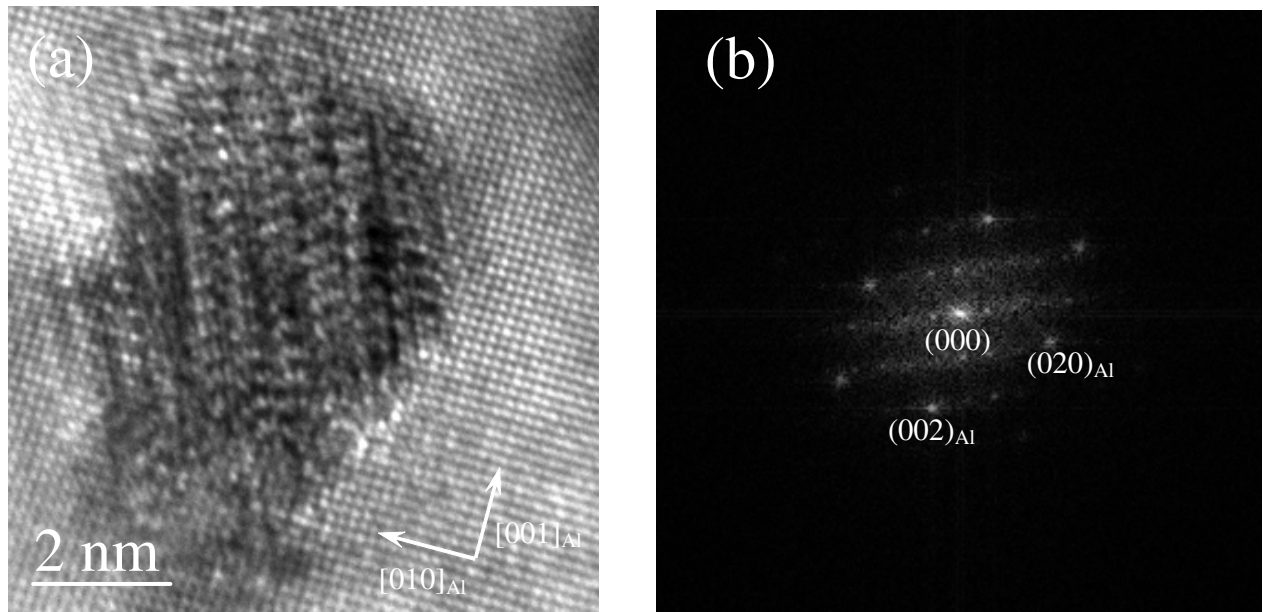


Figure 10: HRTEM image (a) and its Fourier transform (b) of a precipitate of the S' phase observed in alloy 1 after water quenching and ageing for 15h at 180°C.